Filler-induced composition waves in phase-separating polymer blends

Benjamin P. Lee,* Jack F. Douglas,† and Sharon C. Glotzer
Polymers Division and Center for Theoretical and Computational Materials Science, National Institute of Standards and Technology, Gaithersburg, Maryland 20899
(Received 28 April 1999)

The influence of immobile filler particles (spheres, fibers, platelets) on polymer-blend phase separation is investigated computationally using a generalization of the Cahn-Hilliard-Cook (CHC) model. Simulation shows that the selective affinity of one of the polymers for the filler surface leads to the development of concentration waves about the filler particles at an early stage of phase separation in near critical composition blends. These ''target'' patterns are overtaken in late-stage phase separation by a growing ''background'' spinodal pattern characteristic of blends without filler particles. The linearized CHC model is used to estimate the number of composition oscillations emanating from isolated filler particles. In far-off-critical composition blends, an ''encapsulation layer'' grows at the surface of the filler rather than a target pattern. The results of these simulations compare favorably with experiments on filled phase-separating ultrathin blend films in which the filler particles are immobilized on a solid substrate. [S1063-651X(99)12111-1]

PACS number(s): 64.75.+g, 68.55.Jk, 47.54.+r, 61.41.+e

I. INTRODUCTION

The bulk properties of miscible fluid mixtures are characteristically insensitive to their microscopic fluid structure near the critical point for phase separation, where the properties are governed by large-scale fluctuations in the local fluid composition. Composition fluctuations occur similarly for most near-critical fluid mixtures, so that the properties of these fluids are subject to a ''universal'' description. This accounts for the success of simple mathematical models of critical phenomena (e.g., Ising model, ϕ^4-field theory) that contain the minimal physics of these fluctuation processes. Although mixtures near their critical point are susceptible to external perturbations, the influence of microscopic heterogeneities tends to become ''washed out'' in the large-scale fluid properties, apart from changes in critical parameters describing the average properties of the fluid (e.g., critical temperature and composition, apparent critical exponents, etc.). This situation changes, however, when the fluid mixture enters the two-phase region. The fluid is then far from equilibrium and perturbations can grow to have a large-scale influence on the phase-separation morphology. Perturbations in these unstable fluids can be *amplified* rather than washed out at larger length scales. Inevitably, the theoretical description of this kind of self-organization process is complicated by various nonuniversal phenomena associated with the details of the particular model or experiment under investigation [1]. The beneficial aspect of this sensitivity of phase separation and other pattern-formation processes to perturbations is that it offers substantial opportunities to *control* the morphology of the evolving patterns and leads to a great multiplicity of microstructures.

Many previous studies have considered the application of external influences (flow [2] and gravitational [3] fields, concentration [4] and temperature [5] gradients, chemical reactions [6], crosslinking [7,8], etc. [9]) to perturb fluid phase separation, but the investigation of geometrical perturbations is more recent. There have been numerous studies on the perturbation of phase separation arising from the presence of a plane wall, which is one of the simplest examples of a geometrical perturbation of phase separation [10–12]. Measurements and simulations both show the development of ''surface-directed'' composition waves away from plane boundaries under the condition where one component has an affinity for the surface. The scale of these coarsening surface waves grows much like those of bulk phase-separation patterns [10–17]. Recent simulations [18,19] and experiments [18,20–23] have shown that variation of the polymer-surface interaction within the plane of the film allows for the control of the local polymer composition in blends phase separating on these patterned substrates (''pattern-directed phase separation'' [18]). Measurements have also indicated that the polymer-air boundary of phase-separating blend films on patterned substrates can be strongly perturbed by phase separation within the film [23–25] and thermal fluctuations of the polymer-air boundary can also strongly influence the structure of thin polymer films [26].

In the present paper we focus on the consequences of having geometrical heterogeneities of finite extent in a phase-separating blend. The Cahn-Hilliard-Cook (CHC) theory [27] for phase separation is adapted to describe phase separation of a blend with spherical, cylindrical (fiber), and platelike shaped filler particles. The extended dimensions of the fiber and platelet filler particles are taken to be much larger than the scale of the phase-separation process. A variable polymer-surface interaction is incorporated into the filler model in a fashion similar to previous treatments of plane surfaces [13–15].

The paper is organized as follows. In Sec. II we briefly summarize the CHC model to introduce notation, to define the relation between model parameters and those of polymer blends theory, and to explain modifications required for incorporating immobile filler particles into the CHC simulations of phase separation. Section III summarizes the results of simulations for representative situations. Key phenomena

*Permanent address: Department of Physics, Bucknell University, Lewisburg, PA 17837.
†Author to whom correspondence should be addressed.

are identified. (i) Target composition patterns form in near-critical composition blends. (ii) Target patterns are a transient phenomenon. (iii) The scale of the target patterns depends on quench depth and molecular weight. (iv) Qualitative changes in the filler-induced composition patterns occur when the surface interaction is neutral and when the blend composition is off-critical. (v) Multiple filler particles induce composition waves exhibiting complex interference patterns. Section IV provides a simple analytic estimate of the scale of the target pattern based on the linearized CHC theory, and these results are tested against simulations for circular filler particles. In Sec. V, simulation results are compared to experiments on ultrathin polymer films having silica bead filler particles immobilized by the solid substrate on which the films were cast. [Ultrathin blend films are defined to be thin enough ($\leqslant 100$ nm) to suppress phase separation transverse to the solid substrate (''surface directed'' phase separation) so that phase separation occurs quasi-two-dimensionally in the plane of the substrate.] Atomic force microscopy measurements on the filled blend films are compared to the analytical predictions. Simulations of phase separation in off-critical blend films are briefly compared to analogous experiments. Measurements on crosslinked blend films are also considered. The final section discusses generalizations of the present study to manipulate the structure of phase-separating blends.

II. THE MODEL

A. CHC equation

We present a brief discussion of the CHC model [27–29] to introduce notation and to explain the modifications required for incorporating filler particles. The modeling of the phase-separation dynamics is based on gradient flow of a conserved order parameter $\phi(\mathbf{r},t)$,

$$\frac{\partial}{\partial t}\phi(\mathbf{r,t}) = M\nabla^2 \frac{\delta F[\phi]}{\delta \phi(\mathbf{r})} + \zeta(\mathbf{r},t), \tag{2.1}$$

with $\phi(\mathbf{r},t)$ equal to the local volume fraction of one of the blend components. Incompressibility of the mixture is assumed so that the local volume fraction of the second component is $1-\phi$. The mobility M is assumed to be spatially uniform and independent of concentration and the free-energy functional $F[\phi]$ has the general form

$$F[\phi(\mathbf{r})] = \int \frac{d\mathbf{r}}{v}[\tfrac{1}{2}k_B T\kappa(\phi)(\nabla\phi)^2 + f(\phi) - \mu_{\rm eq}\phi], \tag{2.2}$$

where $f(\phi)$ is the bulk Helmholtz free energy per lattice site, v is the volume per lattice site, k_B is Boltzmann's constant, T is temperature, and $\kappa(\phi)$ is a measure of the energy required to create a gradient in concentration. Higher-order gradient terms are neglected. The chemical potential is given by $\mu_{\rm eq} = \partial f/\partial\phi|_{\phi_{\rm eq}}$, which ensures that $\phi(\mathbf{r}) = \phi_{\rm eq}$ is the solution of $\delta F[\phi]/\delta\phi(\mathbf{r}) = 0$. Finally, thermal fluctuations necessary to ensure a Boltzmann distribution of $\phi(\mathbf{r})$ in equilibrium are included via the Gaussian random variable ζ. The average of ζ vanishes, and ζ obeys the relation

$$\langle \zeta(\mathbf{r},t)\zeta(\mathbf{r}',t')\rangle = -2Mk_B T\nabla^2\delta(\mathbf{r}-\mathbf{r}')\,\delta(t-t'). \tag{2.3}$$

For temperatures near the critical temperature T_c, the free energy can be expanded in powers of the composition fluctuation $\psi(\mathbf{r}) = \phi(\mathbf{r}) - \phi_c$, giving the Ginzburg-Landau (GL) functional

$$F[\psi(\mathbf{r})] = k_B T\int \frac{d\mathbf{r}}{v}[\tfrac{1}{2}\kappa_c(\nabla\psi)^2 + \tfrac{1}{2}c\psi^2 + \tfrac{1}{4}u\psi^4 + \cdots], \tag{2.4}$$

where $\kappa_c \equiv \kappa(\phi_c)$. Neglected terms are either higher order in ψ or in $\sqrt{c} \propto \sqrt{T-T_c}$, which is small near the critical point. Equation (2.1), in combination with Eq. (2.4), defines the well-known model B [30],

$$\frac{\partial}{\partial t}\psi(\mathbf{r},t) = -M(k_B T/v)\nabla^2(\kappa_c\nabla^2\psi - c\psi - u\psi^3) + \zeta(\mathbf{r},t). \tag{2.5}$$

Equation (2.5) is used to study the dynamics following a quench to the two-phase region $T<T_c$, where $c<0$. In that case, the CHC equation may be rescaled into the dimensionless form [31]

$$\frac{\partial}{\partial t}\psi(\mathbf{r},t) = -\nabla^2(\nabla^2\psi + \psi - \psi^3) + \epsilon^{1/2}\eta(\mathbf{r},t) \tag{2.6}$$

by making the substitutions

$$\begin{aligned} \mathbf{r} &\to (|c|/\kappa_c)^{1/2}\mathbf{r}, \\ t &\to (Mk_B Tc^2/v\kappa_c)t, \\ \psi &\to (u/|c|)^{1/2}\psi. \end{aligned} \tag{2.7}$$

Note that this amounts to rescaling space by $\sqrt{2}\xi^-$, where ξ^- is the thermal correlation length in the two-phase region, and time by $\tau = D_{\rm coll}/2(\xi^-)^2$, with $D_{\rm coll}$ the collective diffusion coefficient. Here the noise term $\eta(\mathbf{r},t)$ satisfies $\langle\eta(\mathbf{r},t)\rangle = 0$ and the relation

$$\langle\eta(\mathbf{r},t)\,\eta(\mathbf{r}',t')\rangle = -\nabla^2\delta(\mathbf{r}-\mathbf{r}')\,\delta(t-t'). \tag{2.8}$$

The only parameters left to specify the dynamics are the (conserved) average concentration $\psi_0 \equiv \langle\phi\rangle - \phi_c$ and the dimensionless noise strength parameter ϵ,

$$\epsilon = 2u/(\kappa_c^{d/2}|c|^{(4-d)/2}). \tag{2.9}$$

Roughly speaking, the reciprocal of ϵ is a measure of the quench depth. The parameter ϵ also arises in discussions of the width of the critical region, and the connection between thermal noise strength and the Ginzburg criterion was first noted by Binder [32].

B. Polymer blends

For polymer blends we take the Flory-Huggins (FH) form of the Helmholtz free energy per lattice site,

$$\frac{f^{\rm FH}(\phi)}{k_B T} = \frac{\phi}{N_A}\ln\left(\frac{\phi}{N_A}\right) + \frac{1-\phi}{N_B}\ln\left(\frac{1-\phi}{N_B}\right) + \chi\phi(1-\phi). \tag{2.10}$$

Here χ represents the monomer-monomer interaction energy, N_i is the polymerization index of component i, and ϕ is the volume fraction of component A. For the coefficient of the gradient term, we use de Gennes' random-phase approximation (RPA) result (neglecting the enthalpic contribution [28]),

$$\kappa(\phi)=\frac{1}{18}\left[\frac{\sigma_A^2}{\phi}+\frac{\sigma_B^2}{1-\phi}\right], \tag{2.11}$$

where σ_A and σ_B are monomer sizes of the A and B blend components, given in terms of the radius of gyration of the ith component $R_{g,i}$ by $\sigma_i^2=R_{g,i}^2/N_i$.

FH theory exhibits a critical point at

$$\phi_c=N_B^{1/2}/(N_A^{1/2}+N_B^{1/2}),$$

$$\chi_c\equiv\chi(\phi_c,T_c)=[N_A^{1/2}+N_B^{1/2}]^2/(2N_AN_B). \tag{2.12}$$

Consequently, the coefficients of the GL functional are defined as [33]

$$c=2\chi_c(1-\chi/\chi_c),$$

$$u=\frac{4}{3}\chi_c^2\sqrt{N_AN_B},$$

$$\kappa_c=\frac{1}{18}[\sigma_A^2(1+\sqrt{N_A/N_B})+\sigma_B^2(1+\sqrt{N_B/N_A})]. \tag{2.13}$$

The phase-separation dynamics of polymer blends can then be described by the dimensionless CHC equation with ϵ determined by molecular parameters,

$$\epsilon=\frac{36\sqrt{2}f(x)}{\gamma^3(\chi/\chi_c-1)^{1/2}N^{1/2}}, \tag{2.14}$$

where $N_A=N$ and $x=N_B/N, f(x)=(1+\sqrt{x})^3/8x$, and γ is the ratio of monomer size to lattice size,

$$\gamma=\frac{[\sigma_A^2(1+1/\sqrt{x})+\sigma_B^2(1+\sqrt{x})]^{1/2}}{2v^{1/3}}. \tag{2.15}$$

γ simplifies to $\gamma=\sigma_{A,B}/v^{1/3}$ for symmetric blends. Thus we see that deep quenches ($\chi\gg\chi_c$) and high molecular weight polymers effectively reduce the thermal fluctuations in the rescaled dynamical equations.

C. Surface energetics

In the presence of a surface, we add a local surface interaction energy to be integrated over the boundary,

$$F_s[\psi]=\int_S d^{d-1}x[h\psi+\tfrac{1}{2}g\psi^2+\cdots]. \tag{2.16}$$

The coupling constant h in the leading term plays the role of a surface field which breaks the symmetry between the two phases, i.e., attracts one of the components to the filler surface. The coupling constant g in the second term is neutral regarding the phases, and results from the modification of the interaction energy due to the missing neighbors near the surface [34] and chain connectivity [35]. For studies of surface critical phenomena [36,37] and surface dynamics [38,39] one typically keeps only these terms as a minimal model of phase separation with boundaries.

There has been considerable attention given to the subject of the appropriate dynamical equations for the surface boundary conditions [38]. We follow most authors and impose zero flux at the boundary, $\hat{\mathbf{n}}\cdot\mathbf{j}_\psi=0$, which gives

$$\hat{\mathbf{n}}\cdot\boldsymbol{\nabla}(\nabla^2\psi+\psi-\psi^3)=0. \tag{2.17}$$

For the second condition we impose that of local equilibrium at the surface, namely,

$$\hat{\mathbf{n}}\cdot\boldsymbol{\nabla}\psi=h+g\psi. \tag{2.18}$$

While more sophisticated treatments are available [17], they lead to dynamics which rapidly relax to equilibrium and satisfy the above condition. The details of how we implement Eqs. (2.17) and (2.18) in simulations with a curved interface are presented in Appendix A.

D. Simulation details

The equation of motion is solved using a standard central finite difference scheme for the spatial derivatives, and a first-order Euler integration of the time step [40]. In all the simulations, the lattice spacing is taken between 0.7 and 1.0 in dimensionless units (sufficiently smaller than any relevant physical length scales) and the time step is taken sufficiently small to avoid numerical instability. In the present paper, all simulations are performed in $d=2$ on lattices up to size 128^2, depending on the choice of mesh size. We note that the CHC equation is known to exhibit quantitatively similar pattern formation and coarsening kinetics in two and three dimensions. Important differences between 2D and 3D simulations can be expected in the late stage of phase separation, however, where hydrodynamic interactions associated with fluid flow can influence the evolution of the phase-separation pattern (see the discussion in Ref. [25]). The particular choice of 2D simulations is made because the experiments considered below are for ultrathin blend films that should be reasonably approximated as two-dimensional [25] and, of course, the results of the 2D simulations are computationally less demanding and easier to visualize. The analytic theory developed below is notably not restricted to 2D, and filler particles of a general dimensionality (rods, sheets, spheres) are considered. Further technical details about Cahn-Hilliard-type simulations of polymer blends can be found in Ref. [28].

III. ILLUSTRATIVE SIMULATIONS

In Fig. 1 we show the influence of an isolated, immobile, circular filler particle on the development of the phase-separation pattern of a blend film having a critical composition. The thermal noise is small in these two-dimensional simulations ($\epsilon=10^{-5}$), corresponding to high molecular weight and/or a deep quench (low and high temperatures relative to the critical temperature for upper and lower critical solution type phase diagrams, respectively). At an early

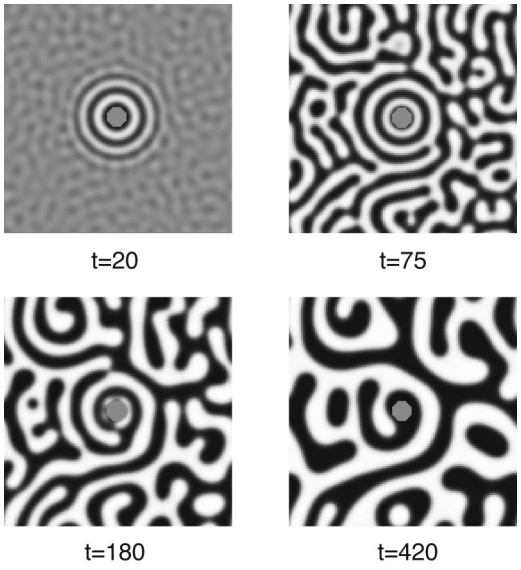

FIG. 1. CHC simulation of the influence of filler particles on polymer-blend phase separation in a critical composition blend. Calculations are performed in $d=2$ with $\epsilon=10^{-5}$, $g=1.0$, and $h=1.0$. In the reduced units of CHC theory [cf. Eq. (2.7)], $R=5.6$ (or in explicit units $R\simeq 3.96\xi^{-}$). The target phase-separation patterns are well developed at early times, but fragment as the ''background'' spinodal phase-separation pattern coarsens to a scale larger than the filler particle (central gray region in the figure). We have verified that the scale of the phase-separation pattern in this simulation grows with a near $t^{1/3}$ power law over the time range indicated in the figure. This growth law is independent of spatial dimension and is characteristic of the intermediate stage of phase separation in blends when hydrodynamic effects are not important.

stage of the phase-separation process, the filler particle creates a spherical composition wave disturbance that propagates a few ''rings'' into the phase-separating medium in which the filler particle is embedded. The target rings initially have the size of the maximally unstable ''spinodal wavelength'' λ_0 obtained from the linearized theory [27]. As the characteristic scale of the bulk phase-separation pattern coarsens to the size of the filler particle, the outer rings of the ''target'' pattern become disconnected and increasingly become absorbed into the background spinodal pattern. The perturbing influence of the particle becomes weak at a late stage of the phase separation where the scale of the background phase-separation pattern exceeds the filler particle size. The finite extent of the filler thus limits the development of the composition waves to a transient regime. The assumption that the filler particles are immobile requires that the scale of particle diffusion is small in comparison to the scale of the phase-separation pattern. This situation may be realized for modest size particles ($\geqslant 100$ nm) in relatively high viscosity blends and in the case of phase separation in blend films where the particles are fixed to the solid substrate (this latter case is discussed in Sec. V).

The formation of target patterns can be described as composition waves propagating into the bulk, unstable region until they are overwhelmed by the developing background spinodal decomposition pattern. The rate of onset of spinodal decomposition is controlled by the strength of thermal fluctuations, hence the noise parameter ϵ plays a crucial role in determining the radial extent of the composition waves. Figure 2 shows two systems with equal surface interaction, but with varying noise strengths: (a) $\epsilon=10^{-3}$ and (b) $\epsilon=10^{-5}$. We see that the spatial extent of the target pattern is larger for smaller ϵ. Consequently, we expect deeply quenched and/or high molecular weight polymer blends to be favorable systems for observing filler-induced composition waves because of the relatively low thermal noise level typical of these systems and the relatively high viscosity of these fluids, which slows the dynamics and makes measurements of intermediate stage patterns possible (e.g., via atomic force microscopy as discussed in Sec. V). In Sec. IV, we use the linearized CHC equation to estimate the extent of the composition wave.

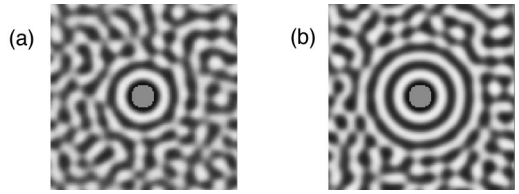

FIG. 2. Composition waves resulting from different values of thermal noise: (a) $\epsilon=10^{-3}$ and time $t=21$ in dimensionless units; (b) $\epsilon=10^{-5}$ and time $t=33$. The surface interaction parameters are $h=1.0$ and $g=0$ for both, and the filler radius is $R=5.6$.

We observe that the composition waves disappear when the particle radius R becomes vanishingly small, and the persistent waves developing from planar surfaces are recovered for very large spherical particles. We then examine particles of sizes intermediate between these extreme limits and during the intermediate phase-separation period in which the target patterns are well developed. Figure 3 shows the angular-averaged composition profile $\psi(z)$, with $z\equiv r-R$ the radial distance from the surface of the filler particle. We observe that the amplitude of the local composition fluctuations becomes more developed and more sharply defined with increasing filler size, R. In comparison to the planar surface ($R\rightarrow\infty$), the composition wave profile for $R=10$ is only slightly reduced in amplitude, whereas for $R=3$ the amplitude is reduced to half that of the wall case. We also remark that the radial extent of the target pattern is similar for all particle sizes.

We next examine the influence of the surface interaction on the formation of filler-induced target patterns. The impact of the symmetry-breaking perturbation of the filler particle on the phase separation may be tuned through the surface

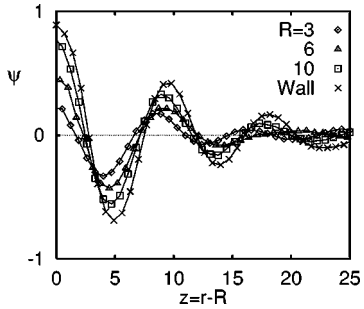

FIG. 3. Typical angular-averaged radial composition profiles $\psi(z)$ for $R=3,10$, and ∞ in an intermediate stage of phase separation. Parameters used are $h=0.1$, $g=0,\epsilon=10^{-2}$, and the time is $t=25$. Averages were taken over ten independent configurations.

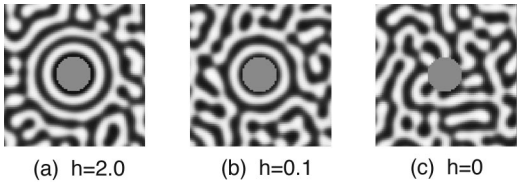

FIG. 4. Influence of surface interaction on filler-induced pattern formation. The figures show intermediate-stage phase separation ($t=50$) with thermal noise $\epsilon=10^{-4}$ and radius $R=9.6$. Filler-induced target pattern for a selective polymer interaction (a) $h=2.0$ and (b) $h=0.1$, and (c) a nonselective polymer interaction, $h=0$. Note the tendency for the domains to align perpendicularly to the neutral filler interface.

interaction parameters g and h. We focus our attention on h since it has a predominant effect on the resulting pattern formation.

Figure 4 shows CHC simulations of blend phase separation for the case where one component strongly prefers the filler, weakly prefers the filler, and has no preference for the filler ($h=0$). The quench depth parameter and computation times are identical in these images. We see that the target patterns do not form in the case of filler particles with a (''neutral'') nonselective interaction, but rather there is a tendency for the patterns to align *perpendicularly* to the interface. This type of compositional alignment, which we find is even more pronounced in the case of a planar surface, also occurs in block copolymer fluids [41]. The perturbing influence of the boundary interaction saturates with an increase of h, as can be seen by comparison of the $h=2.0$ and $h=0.1$ cases. Below we demonstrate that the spatial extent of the target pattern depends logarithmically on h.

Target waves are a variety of spinodal pattern with a symmetry set by the shape of the filler particle boundary. The introduction of surface patterns on a solid substrate can similarly break the symmetry of the phase-separation process and can be used to impart a particular ''shape'' to the spinodal pattern [18,21]. A previous CHC simulation by us considered this ''patterned-directed'' phase separation in near-critical composition blend films [18].

The blend composition can also have a large influence on the character of the filler-induced phase-separation structures in blends, particularly when sufficiently far off critical to suppress the spinodal instability. In this case we find a layer of composition enrichment (''encapsulation layer'') forms about the filler particle, but there are no target patterns [42]. This encapsulation layer grows in time, but appears to grow slower than $t^{1/3}$. A nonselective interaction ($h=0$) leads to the absence of encapsulation by the minority phase, and minority phase nucleation occurs largely unaffected by the presence of the filler. We thus find that the development of target patterns requires the conditions of ordinary spinodal pattern formation (i.e., ''near'' critical composition) and the existence of a heterogeneity to initiate the wave disturbance.

A representative example of the interference between filler-induced rings at a nonvanishing filler concentration is shown in Fig. 5. Filler particles can each have an affinity for the different blend components so that the enriching phase (''charge'') can vary near the surface of the filler particle at the core of the target waves. (Sackmann has noted that composition enrichment patterns occur about membrane proteins in lipid mixtures comprising living cell membranes, and these patterns mediate protein interactions, leading to attractive or repulsive interactions depending on the ''charge'' [43].) In the low noise limit it should be possible to obtain novel wave patterns such as those found in reaction-diffusion models with regularly spaced sources for wave propagation [44], but we do not pursue this here. We do mention that the use of filler particles responsive to external fields could allow the manipulation of the large-scale phase-separation pattern if the external fields are used to align the filler particles.

FIG. 5. Illustrative CHC simulation of blend phase separation with many filler particles. Filler particles preferential to each phase are included (the two filler types have a dark and light filler core). Simulation parameters are $t=80, h=\pm 1.0, R=2.0$, and $\epsilon=10^{-6}$. Note the interference pattern between these composition waves.

IV. ESTIMATION OF THE SPATIAL EXTENT OF THE TARGET PATTERNS

In this section we derive an approximate analytical expression for the spatial extent of the composition wave pattern. Our method is based on the observation above that the composition wave propagates until it is overwhelmed by the growth of the bulk spinodal decomposition background pattern. In the context of surface-directed spinodal decomposition, a qualitative explanation of this type of phenomenon was proposed by Ball and Essery [13], who argued that the early time dynamics can be adequately described by the linearized CHC equation, in which the composition wave and the bulk spinodal decomposition add linearly. Both processes continue independently until a local nonlinear threshold value of $|\psi| \approx \psi_t$ is reached, which then relaxes toward the equilibrium value $\psi=\pm 1$.

We test this conjecture numerically in the case of the filler inclusions. First, we simulate the CHC equation in bulk, with no filler particle, and determine the time t_0 at which the root-mean-square concentration $\langle \psi^2(t) \rangle^{1/2}$ reaches the threshold value $\psi_t=0.15$ (our reason for this choice is given below). Next, we simulate the filled blend *in the absence of noise* solving for the pattern at time t_0, and then estimate the radius r_0 at which the composition wave (envelope) exceeds ψ_t. Finally, we perform the simulation with *both* the filler particle and the thermal noise, and find the pattern to be

well-characterized by the size r_0 for a range of noise and surface interaction parameters.

Based on these ideas, we next develop an analytic estimate of the spatial extent of the pattern using the linearized CHC theory [27]. At early times the order parameter does not deviate significantly from zero, and one linearizes Eq. (2.6) to obtain

$$\partial_t \psi = -\nabla^2(k_0^2+\nabla^2)\psi + \epsilon^{1/2}\eta, \tag{4.1}$$

where $k_0^2 = 1-3\psi_0^2$. We apply this equation first to the determination of the root-mean-square order parameter $\psi_{\rm rms}(t) \equiv \langle \psi(t)^2\rangle^{1/2}$, which characterizes the rate of growth of the concentration fluctuations at very early times following a quench to the two-phase region. Fourier transformation gives

$$\partial_t \tilde{\psi}(\mathbf{k},t) = k^2(k_0^2-k^2)\tilde{\psi} + \epsilon^{1/2}\tilde{\eta}(\mathbf{k},t). \tag{4.2}$$

The structure factor $S(\mathbf{k},t) = \langle \tilde{\psi}(\mathbf{k},t)\tilde{\psi}(-\mathbf{k},t)\rangle$ is then

$$S(\mathbf{k},t) = \frac{\epsilon(e^{2k^2(k_0^2-k^2)t}-1)}{2(k_0^2-k^2)}. \tag{4.3}$$

$\psi_{\rm rms}$ is found by integrating $S(\mathbf{k},t)$ with respect to k,

$$\langle \psi^2(t)\rangle = \int \frac{d^d\mathbf{k}}{(2\pi)^d} S(\mathbf{k},t). \tag{4.4}$$

Following [13], we observe that the integrand is sharply peaked about $k = k_0/\sqrt{2}$ and we approximate it by a Gaussian. The integral is then readily evaluated to find (to leading order in $1/t$)

$$\langle \psi^2(t)\rangle = \epsilon\, e^{(1/2)k_0^4 t}\left(\frac{\pi}{2t}\right)^{1/2} \frac{d}{k_0^{4-d}\,\Gamma(1+d/2)(8\pi)^{d/2}}. \tag{4.5}$$

This result, when tested against simulations of the fully nonlinear CHC, agrees well up to $\langle \psi^2(t)\rangle^{1/2} \approx (0.15)$, thus motivating our choice for ψ_t indicated above.

Finally, we equate $\langle \psi^2(t_0)\rangle$ to ψ_t^2 to determine the time t_0 at which the bulk phase-separation process has reached the nonlinear threshold. The resulting transcendental equation for t_0 can be approximately solved by observing that $\psi_t^2/\epsilon \gg 1$ in low noise conditions, and that this ratio must be compensated primarily by the $e^{k_0^4 t_0/2}$ factor. Equating these two and then iteratively improving the estimate of t_0 yields

$$t_0 \approx \frac{2}{k_0^4}\ln\left(\frac{\psi_t^2}{\epsilon}\right) + \ln\left(\frac{2\Gamma(1+d/2)(8\pi)^{d/2}\sqrt{\ln(\psi_t^2/\epsilon)}}{k_0^{d-2}d}\right). \tag{4.6}$$

Next, we consider the linearized theory for the filled blend. We solve Eq. (4.1) for the exterior of the filler particle or fiber, and in the absence of thermal noise (the noise can simply be averaged out of the composition wave within the linearized theory). We consider idealized filler particles that are symmetric and finite in some of their coordinates and infinite (i.e., very large on the phase-separation pattern scale) in the remaining coordinates defining the particle dimensions. With such symmetry, the composition wave depends only on the coordinate perpendicular to the interface, which is a radial coordinate in $d_\perp$ dimensions. For example, a spherical particle in $d=3$ corresponds to $d_\perp = 3$, a cylindrical fiber is prescribed by $d_\perp = 2$, and a platelet filler reduces to the planar surface with $d_\perp = 1$. We can treat the general $d_\perp$ case through the $d_\perp$-dimensional Laplacian,

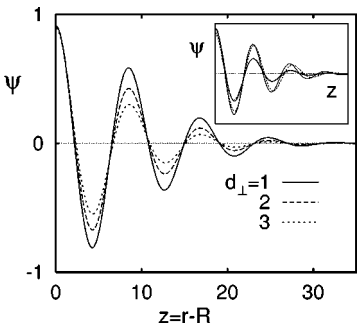

FIG. 6. Influence of particle shape on the development of filler-directed composition waves at early time. Radial composition profiles $\psi(z)$ are obtained from the linearized CHC equation for symmetric particles finite in $d_\perp$ directions, corresponding to platelet fillers ($d_\perp = 1$), fibers ($d_\perp = 2$), and spherical fillers ($d_\perp = 3$). The radius is $R = 10$ and the surface interaction parameters are $h = 0.005$ and $g = 0$. The reduced time is $t = 25$. The inset shows the approximate solutions of Eqs. (4.11) and (4.13) (dashed lines), compared to the $d_\perp = 1$ and 3 numerical solutions from the main figure (solid lines).

$$\nabla^2\psi(r) = \frac{\partial^2\psi}{\partial r^2} + \frac{(d_\perp-1)}{2}\frac{\partial\psi}{\partial r}, \tag{4.7}$$

yielding a fourth-order partial differential equation for Eq. (4.1). The ''source'' for the composition wave comes from the boundary conditions obtained by linearization of Eqs. (2.17) and (2.18), namely

$$\hat{r}\cdot\boldsymbol{\nabla}(k_0^2+\nabla^2)\psi(R) = 0 \tag{4.8}$$

for conservation at the boundary, and

$$\hat{r}\cdot\boldsymbol{\nabla}\psi(R) = h + g\,\psi(R). \tag{4.9}$$

This provides a pseudo-one-dimensional system which can be readily integrated numerically.

The solutions for $d_\perp = 1,2,3$ presented in Fig. 6 illustrate the influence of $d_\perp$ on the composition wave pattern. Increasing $d_\perp$ reduces the amplitude of the composition wave. This feature can be understood to arise from the increasing volume occupied by the outer rings. The opposite situation should hold for *exterior* boundaries having these symmetries, so that more coherent ring structures might be anticipated in phase separation confined to these geometries, especially for spherical cavities. It may prove interesting to examine phase separation in the presence of fractal filler particles (like fumed silica) to determine whether geometry stabilizes or destabilizes the phase-separation pattern and how the evolving phase separation pattern accommodates the fractal boundary structure.

Returning to the analytical estimation of the target pattern size, we expand $\psi(r)$ in a basis which diagonalizes the Laplacian. This amounts to performing a cosine transform for

$d_\perp = 1$, a (J_0) Hankel transform in $d = 2$, and a half-integer Hankel tranform in $d = 3$. The last can be reexpressed as a Fourier cosine transform of $r\psi(r)$ rather than ψ. Here we study the extremal cases of $d_\perp = 1$ and 3, and show that $d_\perp$ has only a minor effect on the pattern size.

First, we revisit the $d_\perp = 1$ case already addressed by Ball and Essery [13]. One can solve Eq. (4.1) with boundary conditions via Fourier cosine transformation with respect to r and Laplace transform with respect to t, with the result

$$\tilde{\psi}(k,s) = \frac{hk^2}{s[s - k^2(k_0^2 - k^2)]} \tag{4.10}$$

for the case $g = 0$ (to which we restrict our attention). Inverting the Laplace transform and using a Gaussian approximation again to invert the Fourier cosine transform gives the solution

$$\psi_{d_\perp = 1}(z,t) \approx \psi(0,t) e^{-(z/4\lambda_0)^2} \cos(z/\lambda_0), \tag{4.11}$$

where $\psi(0,t) \equiv (h/k_0^3)\sqrt{(8/\pi t)}\exp(k_0^4 t/4)$, $\lambda_0^{-1} = k_0/\sqrt{2}$, and where subdominant terms in $1/t$ have been neglected. A nonzero value of g, while complicating Eq. (4.10), would appear in this approximate solution only via the substitution $h \to h + g\psi_0$. In this $d_\perp = 1$ example, the R dependence drops out of the linearized equation, and $z = r$ measures the distance from the wall.

For a given noise strength ϵ we have a time t_0 at which the local composition of one phase reaches ψ_t. For surface interaction h we solve for the distance z_0 out to which the envelope of $\psi(r,t_0)$ exceeds ψ_t. This gives the approximation

$$z_0 \approx 2k_0^3 t_0 \left[1 - \frac{1}{k_0^4 t_0} \ln\left(\frac{k_0^3 \psi_t}{h} \sqrt{\frac{\pi t_0}{8}} \right) \right]. \tag{4.12}$$

Thus, the propagation front grows with a velocity $2k_0^3$ at long times [13], and the terms in square brackets are the leading correction to this long-time asymptotic behavior.

The $d_\perp = 3$ composition profile may be obtained by observing that Eqs. (4.1) and (4.7) yield the same equation for $r\psi_{d_\perp = 3}(z,t)$ as for the composition profile $\psi_{d_\perp = 1}(z,t)$. Thus, we impose the boundary conditions (to leading order in R/r) and follow the above derivation with the result

$$\psi_{d_\perp = 3}(z,t) \approx \frac{R}{R+z} \psi_{d_\perp = 1}(z,t). \tag{4.13}$$

Solving for the value z_0 at which the composition wave envelope equals ψ_t leads to nearly the same expression as the $d_\perp = 1$ case (4.12), with an additional $-\ln(1 + z_0/R)/k_0^4 t_0$ term in the square brackets. Typically $z_0 \lesssim 10R$, k_0 is of order unity, and t_0 ranges from 10 to 30, making this term roughly a 10% correction.

To compare with our simulations, we consider $d_\perp = d = 2$. For z_0 we simply take the arithmetic mean of the values obtained for $d_\perp = 1$ and $d_\perp = 3$ (motivated by numerical solutions). Equation (4.6) for t_0 is substituted into Eq. (4.12) to obtain a prediction for z_0 in terms of h, ϵ, and ψ_0. Here we consider critical quenches with $\psi_0 = 0$, or $k_0 = 1$. Finally, we approximate $\ln t_0$ and $\ln z_0$ with typical values, which introduces less than 10% error with the range of parameters considered here, and thus we obtain

$$z_0 \approx -2.5 - 8.5 \log_{10}\epsilon + 4.6 \log_{10} h. \tag{4.14}$$

A similar expression results for $d = d_\perp = 3$, with the primary difference being a change of the $\log_{10}\epsilon$ coefficient to -7.9.

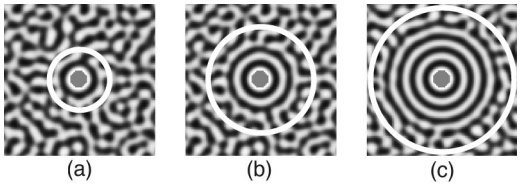

FIG. 7. Comparison between the analytic estimate of the spatial extent of the target pattern and the corresponding CHC simulation at an intermediate stage of phase separation. Simulations are performed at noise levels (a) $\epsilon = 10^{-2}$ corresponding to modest molecular weight and shallow temperature quenches, (b) $\epsilon = 10^{-4}$, and (c) $\epsilon = 10^{-6}$, corresponding to high molecular weight mixtures and deep temperature quenches. The surface interaction $h = 1$ for all cases, the radius $R = 5.6$, and the times for each quench are chosen to correspond to when the spinodal pattern is fully developed: (a) $t = 20$, (b) $t = 30$, and (c) $t = 40$. The solid lines are the predictions of Eq. (4.14).

Figure 7 shows a comparison of this estimate with the simulations. We see that the analytic approximation provides a good rough estimate of the spatial extent of the phase-separation pattern, although it predicts a size typically one oscillation larger than the outermost unbroken target.

We point out that the spherical composition waves are apparent in the average composition profiles even in the rather noisy looking ring patterns found in the late stage of target pattern formation. In Fig. 8 we show a target pattern at intermediate values of noise, as well as the radial average of the composition profile about the center of the target. Comparison shows that the ring composition pattern persists in the radial average even after the target pattern appears visually to have broken up. This provides a possible explanation of the apparent overestimate of the target size in Fig. 7.

V. COMPARISON WITH EXPERIMENTAL RESULTS

While scattering measurements of the growth of composition waves are readily performed for a single plane boundary [11], these measurements become more difficult in filled

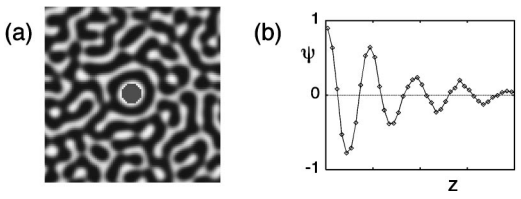

FIG. 8. Late-stage target pattern and corresponding radial composition profile. (a) Filler-induced phase-separation pattern for an intermediate noise value of $\epsilon = 10^{-3}$ at time $t = 35$, $h = 1$, and $R = 5.6$. (b) Averaged radial profile about the center of the filler particle. Note that the ring composition pattern persists in the radial average even after the target pattern appears visually to have broken up.

blends where the filler particles are randomly distributed within the blend. This situation is unfortunate, given the predicted transient nature of the composition wave patterns when the particles are small. However, real space studies of blend phase separation are possible in films sufficiently thin (''ultrathin'') to suppress the formation of surface-directed waves normal to the solid substrate [25]. Under the favorable circumstances that one of the polymer components segregates to both the solid substrate and the polymer-air boundary of these nearly two-dimensional (''ultrathin'') blend films, phase separation is observed within the plane of the film [24,25,45]. The variation of the surface tension in the film accompanying phase separation gives rise to film boundary undulations that can be measured by atomic force microscopy (AFM) and optical microscopy (OM) [25,45]. The thickness of ultrathin blend films is typically restricted to small values ($L \approx 200$ nm) and the height contrast of the surface patterns tends to become larger in still thinner films [23]. A film thickness in the range of 20–50 nm is often suited for observing well resolved phase-separation surface patterns similar to those found in simulations of bulk blends. In the following we compare our results with those of a model blend utilized in ultrathin phase-separation studies reported elsewhere with silica beads added as the model filler [46]. Notably, the filler particles in the experiments associate strongly with the substrate, so they are relatively fixed in place as in our simulations in Sec. III.

The spun-cast films are composed of a near-critical composition blend of polystyrene and poly(vinyl methyl) ether (PVME). The filler particles are silica beads having an average size of about 100 nm, as measured by direct imaging of the particles. This particular filler was chosen because of its tendency to be enriched by polystyrene, rather than PVME, which enriches both the solid and air surfaces. In this way, the filler particles are not competing with the solid or air surfaces for the enriching polymer. Phase separation was achieved by annealing the film approximately 15° within the two-phase region, corresponding to a fairly shallow quench. Film topography (height) was measured by AFM. Further details of the experiment are provided in Ref. [46].

Figure 9 (top) shows the topography of the blend film at an intermediate stage of phase separation where we expect circular filler-induced composition waves to be evident. The pattern resembles the simulated patterns under similar quench conditions. The symmetry of the film phase-separation pattern is locally broken by the presence of the filler particles, leading to the formation of ringlike concentration wave patterns. Note that when observed on a larger scale [Fig. 9 (bottom)], the phase-separation pattern far from any filler particles resembles the typical spinodal decomposition pattern observed in control measurements on the same blends without filler.

It is apparent that the patterns in Fig. 9 are in a relatively late stage of phase separation, where the rings are beginning to break up along with the ''background'' phase-separation pattern. The simulations above indicate that the target patterns are more persistently expressed in the radially averaged patterns, and in Fig. 10 we show the radial average of the AFM height data centered about a representative filler particle. The target pattern in the radially averaged data extends far beyond the ring feature apparent in the image in Fig. 9.

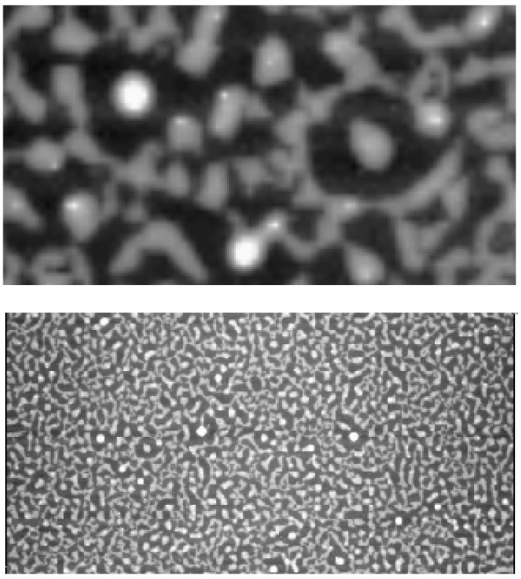

FIG. 9. AFM image of phase-separation pattern in PS/PVME blend film with dilute concentration of filler particles at (top) 20 μm and (bottom) 100 μm scale. The height undulations reflect composition variations within the film associated with surface tension variations [45]. Image contrast has been enhanced by a film washing procedure. From Ref. [46].

The data in Fig. 10 correspond to a shallow quench, and are comparable to the intermediate stage, shallow quench simulation data in Fig. 3.

Next we directly compare the prediction of the linearized theory to the AFM data. An exact solution of $\psi_{d_\perp=2}(z,t)$ is difficult, but we can obtain a reasonable approximation to $\psi_{d_\perp=2}(z,t)$ by generalizing the method described above for $\psi_{d_\perp=1}(z,t)$. We estimate $\psi_{d_\perp=2}(z,t)$ as a Gaussian decay function multiplied by the eigenfunction of the Laplacian in $d=2$ [rather than in $d=1$ as in the case of Eq. (4.11)]. In this approximation, $\psi_{d_\perp=2}(z,t)$ becomes a product of a Gaussian as in Eq. (4.11) and a Bessel function $J_0(2\pi z/\lambda_0)$, and we show a fit of this function to the AFM data in Fig. 10. The fitted value of the particle radius R is 82 nm, which is com-

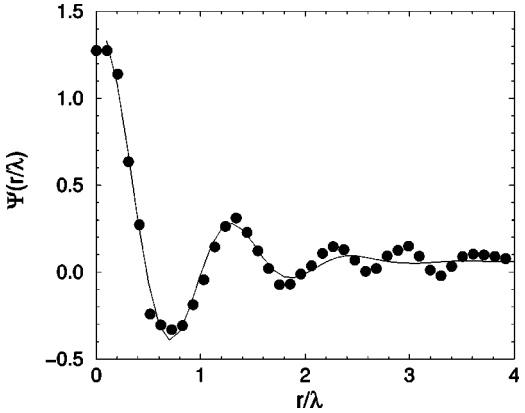

FIG. 10. Radial average of AFM height data centered about an isolated target pattern in Fig. 9. The scale of the damped oscillatory profile is reduced by the phase-separation scale determined by a Fourier analysis of the AFM height data for the entire film. The solid line is a fit to the data as described above. Data from Ref. [46].

parable to the average particle radius obtained by optical microscopy ($R \approx 100$ nm). The scale parameters of the Gaussian and Bessel functions have been adjusted along with the prefactor, which is set by the value of $\psi_{d_\perp=2}(z,t)$ as z tends to zero. It is clear that the oscillatory pattern scale is on the order of the background phase-separation pattern, and that the linearized expression for $\psi_{d_\perp=2}(z,t)$ has the qualitative shape of the measured profile. Such qualitative agreement is the best that can be expected from the linearized theory, which strictly speaking should hold only at very early times.

At still longer times, the phase-separation pattern eventually breaks up into droplets and little difference is observed between the films with and without filler. Thus, the target patterns induced by the filler particles are transient, as observed in the simulations. Of course, the version of the CHC model used here cannot reliably describe quantitative features of these late-stage processes without the incorporation of hydrodynamic interactions.

Under far-off-critical conditions and a selective interaction between the filler particles and one of the polymers ($h > 0$), the filler particles are ''encapsulated'' by a layer of the favored polymer so that concentration waves do not develop. The formation of droplets by nucleation or far-off-critical spinodal decomposition can also have the effect of breaking the symmetry of the phase-separation process, but the pattern formation is not generally the same as for critical composition mixtures. Recent measurements have reported the occurrence of filler encapsulation in a blend of polypropylene and polyamine-6 with glass bead filler particles [8,42]. Encapsulation occurs when the polypropylene-rich phase having the selective interaction for the filler is the minority phase, but no encapsulation occurs when polypropylene is the majority phase. This finding compares well with the simulation results discussed in Sec. IV.

Radiation crosslinking provides another source of heterogeneity that can be introduced readily in phase-separating films. Measurements of irradiated photoreactive blends of PVME and PS with a crosslinkable side group styrene-chloromethyl styrene random copolymer (PSCMS) show the formation of striking ring composition patterns [47,48] and we reproduce one of these patterns in Fig. 11 (compare with Fig. 5). Furukawa [49] has interpreted these observations in terms of a model by which irradiation first brings the blend into the nucleation regime where droplets phase-separate, followed by the entrance into the spinodal regime where the droplets act like the filler particles discussed in the present paper. This is a plausible interpretation of the qualitative origin of these patterns, but it is difficult to interpret these measurements directly from CHC simulations since crosslinking imparts a nontrivial viscoelasticity to the polymer blend [50]. The crosslinking, which also increases the molecular weight of PSCMS, and the increased elasticity both lead us to expect a decrease in the thermal noise and thus an increased tendency to form target patterns. It also seems plausible to us that the crosslinks themselves provide the source of heterogeneity, inducing the development of composition waves.

VI. DISCUSSION

The presence of filler particles in a phase-separating fluid mixture is found to give rise to transient composition wave patterns in simulations based on the Cahn-Hilliard-Cook model and in measurements [46] on ultrathin polystyrene/poly(vinylmethyl) ether blend films with silica filler particles. In both the simulation and the experiment, the composition wave patterns were found to be transient and the filler is found to have a diminishing effect as the scale of the phase-separation pattern becomes larger than the filler particles. The propagation of composition waves is enhanced at lower thermal noise level so that the effect propagates to larger distances for deeper quenches and higher molecular weight blends. The finite size and the dimensionality of the filler particles are found in our simulations to have a similar effect in determining the stability of the composition wave pattern at intermediate times. The composition waves become more stable for particles large in comparison to the spinodal wavelength, and the concentration waves exhibited by these larger particles are similar to planar interfaces. The composition waves about the filler particles are more stable for particles extended at great distance along more directions; i.e., surfaces are more stable than long cylinders, which are more stable than spherical filler particles. Our results compare favorably with experiments on phase-separating filled ultrathin blend films which are nearly two-dimensional, and which contain a relatively low concentration of modest size (radius $\simeq 100$ nm) filler beads fixed to the substrate.

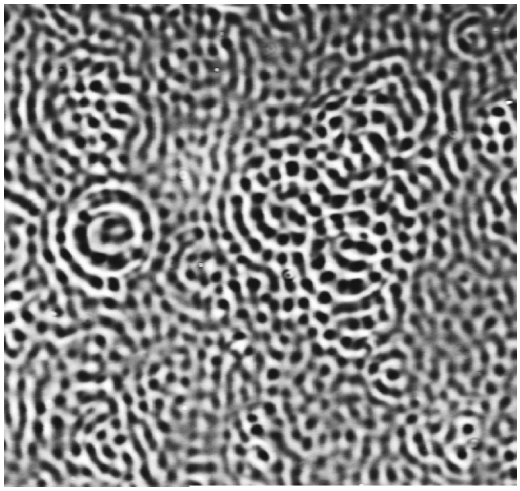

FIG. 11. Phase contrast microscopy image of phase-separation pattern of a photocrosslinked blend. The scale of the image is 10 μm. From [8]. Reproduced with permission from Marcel Dekker.

Filler particles are an example of a perturbation of phase separation by boundaries *interior* to the fluid. It would be interesting to investigate the influence of exterior boundaries of finite extent on phase separation. It seems likely that composition waves within confined geometries should be more stable because of the decreasing surface area of the rings farther from the surface. This should lead to well developed and more long-lasting perturbations of the phase-separation process. The relation between boundary shape and phase-separation morphology should be very interesting for this class of measurements. Phase separation within arrays of filler particles, where the distinction between interior and exterior boundaries becomes blurred and where larger perturbations of the phase-separation process may be anticipated, should also prove interesting. The distinction between

large and small and fixed and mobile filler particles should lead to a range of new phase-separation morphologies since the development of composition waves should lead to changes in the filler-filler interaction that can influence the subsequent development of the film structure. The utilization of geometrically and chemically patterned surfaces and additives offers many opportunities for the control of the phase-separation morphology and resulting properties of blend films, and the study of these surface-induced phase-separation processes raises many interesting problems of fundamental and practical interest.

ACKNOWLEDGMENTS

The present work has benefited greatly from close collaboration with experimentalists in the Polymer Blends Group at NIST. The simulations and experimental work were conducted simultaneously, and we thank Alamgir Karim and Eric Amis for many suggestions which influenced the design and interpretation of our simulations. We thank Giovanni Nisato for many useful conversations and providing the correlation function data for the filled films (Fig. 10). We have also benefited from conversations with Qui Tran-Cong regarding the relation of his measurements to our simulations and for contributing Fig. 11. B.P.L. acknowledges the support of the National Research Council/NIST.

APPENDIX: BOUNDARY CONDITIONS ON A CURVED SURFACE

Curved boundaries complicate the implementation of boundary conditions in a spatially discretized simulation. In the present work, we use a square lattice and simulate filler particles with circular, cylindrical, and spherical symmetry. This requires a method of incorporating the boundary conditions that minimizes the effects of errors caused by approximating curved boundaries by lattices. In this appendix we present our approach to this problem.

Generally, Eqs. (2.17) and (2.18) are imposed by inclusion of ψ and $\mu=-\nabla^2\psi-\psi+\psi^3$ values at the lattice sites on the immediate interior of the boundary (within the wall or filler), which are determined from the boundary conditions before each time step. We superimpose the circular boundary over the square lattice so that no lattice vertices lie along the boundary. Consequently, every interior point corresponds to one of two possibilities, shown as the lower left corners of Figs. 12(a) and 12(b). The boundary condition at the point (x_0,y_0) (shown as a black dot) is not set at the interior lattice site but rather at the intersection of the boundary and the radius passing through the interior lattice site.

In both cases of Fig. 12, we use the three vertices shown as open circles for the discretized representation of $\psi(x_0,y_0)$ and its normal derivative $\hat{\mathbf{r}}\cdot\nabla\psi(x_0,y_0)$. To highest order these representations are unique [holding to $O(\Delta x^2)$ for ψ and $O(\Delta x)$ for the derivative, with Δx the lattice spacing]. Hence, Eq. (2.18) may be used to determine $\psi_{i,j}$, the field at the interior site, from the appropriate exterior points. We find for case (a) the relation

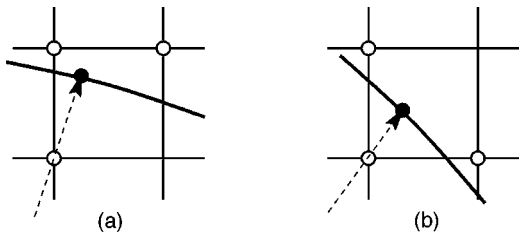

FIG. 12. A curved boundary passes through either adjacent or opposite sides of a lattice unit cell. For both cases we express the field and its normal derivative at (x_0,y_0), the solid dot, in terms of the values at the three vertices depicted by open circles. The dashed line is the radius of the boundary arc.

$$\psi_{i,j}=\frac{(1-g\ell)[(\sin\theta-\cos\theta)\psi_{i,j+1}+\cos\theta\psi_{i+1,j+1}]-h\Delta x}{(1-g\ell)\sin\theta+g\Delta x}, \tag{A1}$$

where ℓ is the distance from the interior lattice site to (x_0,y_0) while θ is the angle between the radius and the horizontal axis. For case (b) the analogous expression is

$$\psi_{i,j}=\frac{(1-g\ell)[\cos\theta\psi_{i+1,j}+\sin\theta\psi_{i,j+1}]-h\Delta x}{(1-g\ell)(\cos\theta+\sin\theta)+g\Delta x}. \tag{A2}$$

The chemical potential $\mu_{i,j}$ may also be assigned at the interior point, in practice by assigning a value to $(\nabla^2\psi)_{i,j}$ to supplement the Laplacian derived from ψ outside the boundary. In this way we can impose the conservation requirement (2.17) for case (a) via

$$\mu_{i,j}=(1-\cot\theta)\mu_{i,j+1}+\cot\theta\mu_{i+1,j+1}, \tag{A3}$$

while for case (b),

$$\mu_{i,j}=\frac{\cos\theta}{\cos\theta+\sin\theta}\mu_{i+1,j}+\frac{\sin\theta}{\cos\theta+\sin\theta}\mu_{i,j+1}. \tag{A4}$$

In simulations with thermal noise we assume a separation of time scales between thermal fluctuations and order-parameter variations (as described in [15]), and simply supplement the above conditions with the conservation law for fluctuations at the boundary: $\hat{\mathbf{r}}\cdot\boldsymbol{\nu}=0$, where ν is the noise current derived from $\eta=\nabla\cdot\boldsymbol{\nu}$.

[1] J. Langer, in *Critical Problems in Physics*, edited by V. L. Fitch, D. R. Marlow, and M. Dementi (Princeton University Press, Princeton, NJ, 1997), pp. 11–27.

[2] T. Hashimoto, K. Matsuzaka, E. Moses, and A. Onuki, Phys. Rev. Lett. **74**, 126 (1996); T. Ohta, H. Nozaki, and M. Doi, J. Chem. Phys. **93**, 2664 (1990); A. Onuki, Int. J. Thermophys. **16**, 381 (1995); C.K. Chan, F. Perrot, and D. Beysens, Phys. Rev. A **43**, 1826 (1991); F. Corberi, G. Gannella, and A. Lamura, Phys. Rev. Lett. **81**, 3852 (1998); Y. Wu, H. Skrola, T. Lookman, and S. Chen, Physica A **239**, 428 (1997); Z. Mitov

and E. Kumachera, Phys. Rev. Lett. **81**, 3427 (1998); A. Frischknecht, Phys. Rev. E **58**, 3495 (1998).
[3] A.M. Lacasta, A. Hernandez-Machado, and J.M. Sancho, Phys. Rev. B **48**, 9418 (1993); K-W To, and C-K Chan, Europhys. Lett. **19**, 311 (1992).
[4] Y. Jayalakshmi, B. Khalil, and D. Beysens, Phys. Rev. Lett. **69**, 3088 (1992); A.M. Lacasta, J.M. Sancho, and C. Yeung, Europhys. Lett. **27**, 291 (1994).
[5] H. Tanaka and T. Sigehuzi, Phys. Rev. Lett. **75**, 874 (1995); J. Kumaki, T. Hashimoto, and S. Granick, *ibid.* **77**, 1990 (1996); J.K. Platten and G. Chaprepeyer, Phys. Lett. A **174**, 325 (1993).
[6] S.C. Glotzer, E.A. DiMarzio, and M. Muthukumar, Phys. Rev. Lett. **74**, 2034 (1995); S.C. Glotzer and A. Coniglio, Phys. Rev. E **50**, 4241 (1994); J.J. Christensen, K. Elder, and H.C. Fogedby, *ibid.* **54**, R2212 (1996); M. Motoyama, J. Phys. Soc. Jpn. **65**, 1894 (1996); S. Puri and H.L. Frisch, J. Phys. A **27**, 6027 (1994).
[7] S.C. Glotzer, M.F. Gyure, F. Sciortino, A. Coniglio, and H.E. Stanley, Phys. Rev. Lett. **70**, 3275 (1993); Phys. Rev. E **49**, 247 (1994).
[8] Q. Tran-Cong, in *Structure and Properties of Multiphase Polymeric Materials*, edited by T. Araki, Q. Tran-Cong, and M. Shibayama (Marcel Dekker, New York, 1998).
[9] C. Yeung, T. Rogers, A. Hernandez-Machado, and D. Jasnow, J. Stat. Phys. **66**, 1071 (1992).
[10] R.A.L. Jones, L.J. Norton, E.J. Kramer, F.S. Bates, and P. Wiltzius, Phys. Rev. Lett. **66**, 1326 (1991).
[11] G. Krausch, C.A. Dai, E.J. Kramer, and F. Bates, Phys. Rev. Lett. **71**, 3669 (1993).
[12] F. Bruder and R. Brenn, Phys. Rev. Lett. **69**, 624 (1992).
[13] R.C. Ball and R.L.H. Essery, J. Phys.: Condens. Matter **2**, 10 303 (1990).
[14] K. Binder and H.L. Frisch, Z. Phys. B: Condens. Matter **84**, 403 (1991).
[15] J.F. Marko, Phys. Rev. E **48**, 2861 (1993).
[16] G. Krausch, C.A. Dai, E.J. Kramer, and F.S. Bates, Ber. Bunsenges. Phys. Chem. **98**, 446 (1994); G. Krausch, C.A. Dai, E.J. Kramer, J.F. Marko, and F.S. Bates, Macromolecules **26**, 5566 (1993).
[17] S. Puri and K. Binder, Phys. Rev. A **46**, R4487 (1992); Phys. Rev. E **49**, 5359 (1994).
[18] A. Karim, J.F. Douglas, B.P. Lee, S.C. Glotzer, J.A. Rogers, R.J. Jackman, E.J. Amis, and G.M. Whitesides, Phys. Rev. E **57**, R6273 (1998).
[19] L. Kielhorn and M. Muthukumar, J. Chem. Phys. **111**, 2259 (1999).
[20] G. Krausch, E.J. Kramer, M.H. Rafailovich, and J. Sokolov, Appl. Phys. Lett. **64**, 2655 (1994).
[21] M. Botan, S. Walheim, J. Mlynek, G. Krausch, and U. Steiner, Nature (London) **399**, 877 (1998).
[22] B.D. Ermi, G. Nisato, J.F. Douglas, J.A. Rogers, and A. Karim, Phys. Rev. Lett. **81**, 3900 (1998).
[23] G. Nisato, B.D. Ermi, J.F. Douglas, and A. Karim, Macromolecules **32**, 2356 (1999).
[24] A. Karim, T.M. Slawecki, S.K. Kumar, J.F. Douglas, S.K. Satija, C.C. Han, T.P. Russell, Y. Liu, R. Overney, J. Sokolov, and M.H. Rafailovich, Macromolecules **31**, 857 (1998).
[25] L. Sung, A. Karim, J.F. Douglas, and C.C. Han, Phys. Rev. Lett. **76**, 4368 (1996).
[26] R. Xie, A. Karim, J.F. Douglas, C.C. Han, and R.A. Weiss, Phys. Rev. Lett. **81**, 1251 (1998).
[27] J.W. Cahn and J.E. Hilliard, J. Chem. Phys. **28**, 258 (1958); **31**, 688 (1959); J.W. Cahn, Acta Metall. **9**, 795 (1961); **10**, 179 (1962); J. Appl. Phys. **34**, 3581 (1963); General Electric Research Lab. Report No. RL 3561M (1964); Acta Metall. **14**, 1685 (1966); Trans. Metall. Soc. AIME **242**, 166 (1986).
[28] S.C. Glotzer, in Annu. Rev. Comput. Phys. **2**, 1 (1995).
[29] A.J. Bray, Adv. Phys. **43**, 357 (1994); H. Furukawa, *ibid.* **34**, 703 (1983).
[30] P.C. Hohenburg and B.I. Halperin, Rev. Mod. Phys. **49**, 435 (1977).
[31] M. Grant *et al.*, Phys. Rev. B **31**, 3027 (1985).
[32] K. Binder, J. Chem. Phys. **79**, 6387 (1983); Phys. Rev. A **29**, 341 (1984).
[33] The chemical potential $\mu_A - \mu_B = \mu_{\rm eq}$ is often omitted in Eq. (2.2), but is generically nonzero, except in the special case of $N_A = N_B$ and $\phi = \phi_c$.
[34] D.L. Mills, Phys. Rev. B **3**, 3887 (1971); K. Binder, Phase Transit. **8**, 1 (1983).
[35] K.F. Freed, J. Chem. Phys. **105**, 10 572 (1996); P.V. Brazhnik, K.F. Freed, and H. Tang, *ibid.* **101**, 9143 (1994).
[36] H.W. Diehl, in *Phase Transitions and Critical Phenomena*, edited by C. Domb and J. L. Lebowitz (Academic, London, 1986), p. 75.
[37] S. Dietrich, in *Phase Transitions and Critical Phenomena*, edited by C. Domb and J. L. Lebowitz (Academic, London, 1988), p. 1.
[38] For a review, see S. Puri and H.L. Frisch, J. Phys.: Condens. Matter **9**, 2109 (1997).
[39] H.W. Diehl and H.K. Janssen, Phys. Rev. A **45**, 7145 (1992).
[40] W. H. Press, B. P. Flannery, S. A. Teukolsky, and W. T. Vetterling, *Numerical Recipes* (Cambridge University Press, New York, 1989).
[41] G.J. Kellogg, D.G. Walton, A.M. Mayes, P. Lambooy, T.P. Russell, P.D. Gallagher, and S.K. Satija, Phys. Rev. Lett. **76**, 2503 (1996); L. Rockford, Y. Liu, P. Mansky, T.P. Russell, M. Yoon, and S.G.J. Mochrie, *ibid.* **82**, 2602 (1999).
[42] D. Benderley, A. Siegmann, and M. Narkis, J. Polym. Eng. **17**, 461 (1997).
[43] E. Sackmann, in *Synergetics — From Microscopic to Macroscopic Order*, edited by E. Frehland (Springer-Verlag, New York, 1984), pp. 68–79.
[44] O. Steinbock, P. Kettunen, and K. Showalter, Science **269**, 1859 (1995).
[45] B.D. Ermi, A. Karim, and J.F. Douglas, J. Polym. Sci. Part B: **36**, 191 (1998).
[46] A. Karim, J. F. Douglas, G. Nisato, D-W. Liu, and E.J. Amis, Macromolecules **32**, 5917 (1999).
[47] T. Tamai, A. Imagawa, and Q. Tran-Cong, Macromolecules **27**, 7486 (1994).
[48] Q. Tran-Cong and A. Harada, Phys. Rev. Lett. **76**, 1162 (1996).
[49] H. Furukawa, J. Phys. Soc. Jpn. **63**, 3744 (1994).
[50] A. Onuki and H. Nishimori, Phys. Rev. B **43**, 13 649 (1991).